JGR Atmospheres

RESEARCH ARTICLE
10.1029/2022JD037436

Assessing Precipitation Over the Amazon Basin as Simulated by a Storm-Resolving Model

L. Paccini[1,2] **and B. Stevens**[1]

[1]Max Planck Institute for Meteorology, Hamburg, Germany, [2]Now at University of Virginia, Charlottesville, VA, USA

Key Points:

- An explicit representation of convection enables the emergence of organized systems (OCS) leading to improved simulations of Amazon rainfall
- Propagating cold-pools and strong low-level easterlies are related to the occurrence of diurnal and nocturnal OCS, respectively
- Systematic biases in the size, intensity and nocturnal precipitation phase of OCS are insensitive to a twofold refinement in resolution

Supporting Information:

Supporting Information may be found in the online version of this article.

Correspondence to:

L. Paccini,
lpaccini@virginia.edu

Citation:

Paccini, L., & Stevens, B. (2023). Assessing precipitation over the Amazon basin as simulated by a storm-resolving model. *Journal of Geophysical Research: Atmospheres*, *128*, e2022JD037436. https://doi.org/10.1029/2022JD037436

Received 4 JUL 2022
Accepted 25 JAN 2023

Author Contributions:

Conceptualization: L. Paccini
Formal analysis: L. Paccini
Funding acquisition: B. Stevens
Investigation: L. Paccini
Methodology: L. Paccini
Supervision: B. Stevens
Visualization: L. Paccini
Writing – original draft: L. Paccini
Writing – review & editing: L. Paccini, B. Stevens

Abstract In this study, we investigate whether a better representation of precipitation in the Amazon basin arises through an explicit representation of convection and whether it is related to the representation of organized systems. In addition to satellite data, we use ensemble simulations of the ICON-NWP model at storm-resolving (2.5–5.0 km) scales with explicit convection (E-CON) and coarse resolutions, with parameterized convection (P-CON). The main improvements in the representation of Amazon precipitation by E-CON are in the distribution of precipitation intensity and the spatial distribution in the diurnal cycle. By isolating precipitation from organized convective systems (OCS), it is shown that many of the well simulated precipitation features in the Amazon arise from the distribution of these systems. The simulated and observed OCS are classified into 6 clusters which distinguish nocturnal and diurnal OCS. While the E-CON ensembles capture the OCS, especially their diurnal cycle, their frequency is reduced compared to observations. Diurnal clusters are influenced by surface processes such as cold pools, which aid to the propagation of OCS. Nocturnal clusters are rather associated with strong low-level easterlies, possibly related to the Amazonian low-level jet. Our results also show no systematic improvement with a twofold grid refinement and remaining biases related to stratiform features of OCS suggest that yet unresolved processes play an important role for correctly representing precipitating systems in the Amazon.

Plain Language Summary The Amazon basin is a relevant element of the Earth system because it influences the global water and carbon cycle, as well as it constitutes a unique ecosystem. Over this important region, conventional climate models do not simulate basic features of rainfall given their inability to resolve this physical process due to their coarse spatial resolution. In this study, we use high-resolution simulations that allow an explicit representation of such physical process (moist convection) and compare them with a set of coarse-resolution simulations and observed precipitation. We find that improvements in the representation of Amazon rainfall, such as the distribution of light and high intensity rain rates, as well as the spatial variability of the diurnal cycle, are explained by the explicit representation of moist convection. Moreover, these improvements arise from the representation of big and organized systems that produce intense rainfall (OCS). We find that particular environmental conditions are associated with the OCS according to their time of occurrence. Diurnal OCS are mainly influenced by interactions with the surface, while nocturnal OCS are related to strong low-level winds. Some of the remaining discrepancies with observed OCS do not show improvements when refining the grid by a factor of two.

1. Introduction

The Amazon basin is the largest rainforest in the Earth and of great relevance for the global hydro-climate and biodiversity (Marengo, 2006; Phillips et al., 2008). It is also a region, like many in the tropics, where climate model precipitation biases are both large and systematic. These biases are evident in every aspect of the representation of precipitation, from its spatial and temporal distribution, to its intensity and form. Models systematically have too little precipitation over the northern Amazon (e.g., Fiedler et al., 2020; Yin et al., 2013). The diurnal cycle is characterized by a too early precipitation peak (Betts & Jakob, 2002; Tang et al., 2021) and evidence of convective organization (Mapes & Neale, 2011), which has been estimated to account for up to 50% of the total Amazon rain (Feng et al., 2021), is effectively absent. In this study, we use kilometer-scale "storm-resolving" simulations over large domains to assess the degree to which they reduce these biases and the extent to which this depends on the explicit representation of organized convective systems (OCS). In doing so our premise is that convective features which are not improved, or for which remaining biases show no clear sign of improvement with increases in resolution, are indicative of an important role for non-convective, for example, cloud microphysical, small (sub hectometer) scale mixing or land-surface processes.

The distinguishing characteristic of storm-resolving models is that they explicitly represent the transient dynamics of convective storm systems, whose length-scales are commensurate with the depth of the troposphere (Satoh et al., 2019). Representing these features become possible at grid spacings of 5–10 km although there is considerable evidence that convection is increasingly distorted as grid spacings increase above 1–2 km. Nonetheless, the ability to represent convective entities as geometric objects that interact dynamically with their environment and are governed by the correct physical relations (laws of motion) seems to explain why even on 5–10 km grid meshes, an explicit representation of convection leads to more physical representations of convection than what is possible using convective parameterization (e.g., Birch et al., 2015; Love et al., 2011). In recent years, storm-resolving models have shown systematic improvements in representing precipitation, albeit to a degree that seems to vary from place to place. For instance, Arnold et al. (2020) found regional differences in the mean precipitation of a 40-day global simulation, where precipitation is overestimated over Africa but underestimated over the Great Plains in North America. While the shortness of the simulations (40 days) and the remote influence of larger-scale biases might explain this discrepancy, they also found that precipitation tends to peak earlier than observations over regions dominated by local thermodynamic forcing; whereas the largest improvements were found in regions where the diurnal cycle is driven by non-local propagating convection.

Although storm-resolving models overcome the long-standing "drizzle" problem of convective parameterizations (Stephens et al., 2010), they still disagree in the representation of high intensity precipitation rates (>80 mm d^{-1}), which is strongly overestimated (Becker et al., 2021) in some models, and apparently underestimated in others (Arnold et al., 2020; Judt & Rios-Berrios, 2021). High intensity precipitation can be related to OCS which we expect storm-resolving models to better represent as compared to models dependent on parameterized convection (e.g., Stevens et al., 2020). How much improvements in the representation of precipitation relate to the representation organized convection is not evident and has not been investigated yet.

A few studies have begun evaluating the representation of precipitation over the Amazon basin using global storm-resolving models. For example, Inoue et al. (2021) compared the semi-diurnal cycle of precipitation with observations for a 5-day period at 3.5 km grid spacing. They found that the model captures the semi-diurnal variation of precipitation in the Amazon basin but it tends to overestimate their amplitudes, especially the second peak during the early morning. Arnold et al. (2020) also analyzed a set of global simulations and found a larger simulated amplitude than observed at a reduced grid spacing (3.5 km). However, in contrast to Inoue et al. (2021), their model did not capture the phase of the precipitation diurnal cycle in the Amazon.

For the most part, storm-resolving model simulations at the regional scale have not been able to look at precipitation over the Amazon in its entirety. For instance, Santos et al. (2019) used a small domain enclosing the city of Manaus and a grid scale of about 780 m. They found that seasonal floods can enhance the intensity of river circulations during daytime and hence convection. Over the eastern Amazon at a grid spacing of 1.5 km, Herbert et al. (2021) analyzed the impact of biomass burning on the diurnal cycle of precipitation. They found that convection is suppressed in the afternoon but enhanced overnight due to aerosol-radiation interactions. Another recent study by Tai et al. (2021), investigated the influence of data assimilation on regional modeling of Amazon precipitation. They performed a 30-day simulation at 4 km grid spacing and focused the analysis on the central Amazon. Their study highlights the improved representation of spatial variability in the precipitation diurnal cycle in contrast to a standard climate model. This feature is related to the representation of OCS which are absent in models reliant on convective parameterization.

In this study we perform storm-resolving simulations with the ICON model over a large domain to study the representation of precipitation over the Amazon. In contrast to previous regional modeling studies, we focus on the Amazon basin in its entirety and, unlike month-long simulations with global models, we perform an ensemble of 30-day simulations at 2.5 and 5 km grid-spacing. Simulations are performed during March as this is the month with the largest convective activity (e.g., Rehbein et al., 2018). For this period we document the ability of storm-resolving simulations to capture the multi-faceted properties of precipitation as observed over the Amazon, in comparison with a model that arguably uses the most efficient, and certainly well calibrated, statistical representation of convection, that is, that developed by Bechtold (2017) for the Integrated Forecast System (IFS) of the European Center for Medium-range Weather Forecasts. We especially focus on the role of organized convection in improving the representation of precipitation and the extent to which this is coupled to particular environmental conditions. By using two resolutions we further infer to what extent remaining deficits in the representation of precipitation are likely to be improved by modest (factor of 2) refinements in resolution.

This question becomes interesting in light of proposals to develop climate information systems based on global models with grid meshes of roughly 1 km (Slingo et al., 2022) as it helps identify the problems that km-scale global models are likely to solve, and those whose solution might require improvements in the representation of processes that remain unresolved, or severely distorted, even on global km-scale meshes.

2. Data and Methodology

2.1. Observed Precipitation

We use the Climate Prediction Center Morphing Method (CMORPH; Xie et al., 2017) dataset for the period from 2010 to 2019. This product estimates precipitation based on passive microwave instruments. The main advantages of CMORPH data are its high temporal (30 min) and spatial (8 km) resolutions. Previous studies have validated its good performance over the Amazon region (e.g., Janowiak et al., 2005). We also tested other high-resolution dataset and similar results were obtained (not shown); therefore we chose the CMORPH data.

2.2. CMIP6

We use simulations from the Coupled Model Inter-comparison Project: Phase 6 (CMIP6; Eyring et al., 2016). Multi-model ensemble means are used from the historical simulations of the 21st century (2000–2014) and are the same used in Fiedler et al. (2020). We use daily and 3-hourly data available from 14 and 13 models, respectively. Simulations were spatially interpolated to the common T63 grid (about 180 km), the native grid of MPI-ESM low-resolution configuration. For a detailed list of the models, the reader is referred to the Supporting Information of Fiedler et al. (2020). Model output from the CMIP6 ensemble only serves as a reference of an average performance of convective parameterizations by state-of-the-art climate models and their simulation of precipitation in the Amazon region.

2.3. ICON-NWP

We use the Icosahedral Nonhydrostatic (ICON) atmospheric model (Zängl et al., 2015) in the numerical weather prediction (NWP) configuration, version 2.3.03. Among the applied physical parameterizations by this model, the parameterization of moist convection is only used for the coarser grid spacing in our experiments (see details in Section 2.3.1). It consists of a bulk mass-flux scheme (Bechtold, 2017), which is one of the latest implementations in NWP of the European meteorological services, the IFS. Other parameterizations common to all simulations are as follow. The radiation scheme uses the Rapid Radiative Transfer Model (RRTM; Mlawer et al., 1997). The parameterization of microphysics is based on a single-moment scheme (Doms et al., 2011), including the prediction of graupel. Turbulent mixing follows a turbulent kinetic energy scheme (Raschendorfer, 2001), which consists of two components that describe the free troposphere and the surface layer, respectively. Also, the ICON-NWP model uses the interactive multi-layer land surface scheme TERRA (Heise et al., 2006). More details about these parameterizations are described in Zängl et al. (2015).

As initial conditions for the simulations we use the operational analysis data from the European Center for Medium-Range Weather Forecasts (ECMWF) - IFS, and from the Hadley Center Sea Ice and Sea Surface Temperature Center (HadISST; Rayner et al., 2003) for SST. Grids and external parameters (e.g., land properties, topography) are retrieved from the Online Grid Generator tool from the German Meteorological Service (DWD) (Web Services of Deutscher Wetterdienst, 2021). This web interface uses the ICON tools version 2.4.13 (Prill, 2020) and software tool EXTPAR (External Parameter for Numerical Weather Prediction and Climate Application) (Asensio et al., 2020) for providing grids and external parameters, respectively.

2.3.1. Experimental Set-Up

We conduct a set of simulations using the same approach as Paccini et al. (2021), in which the experimental configuration has been previously tested. Global simulations, at 40 km grid spacing are called the P-CON simulations and serve as initial and boundary conditions to the one-way nested domains at finer grid spacing. The three inner domains have the convective parameterization switched off considering that using explicit convection from 25 km grid spacing is not inadequate (Vergara-Temprado et al., 2020). Those simulations are called the E-CON simulations. The horizontal resolution of the inner domains is successively increased from 20 km (95°W–35°E,

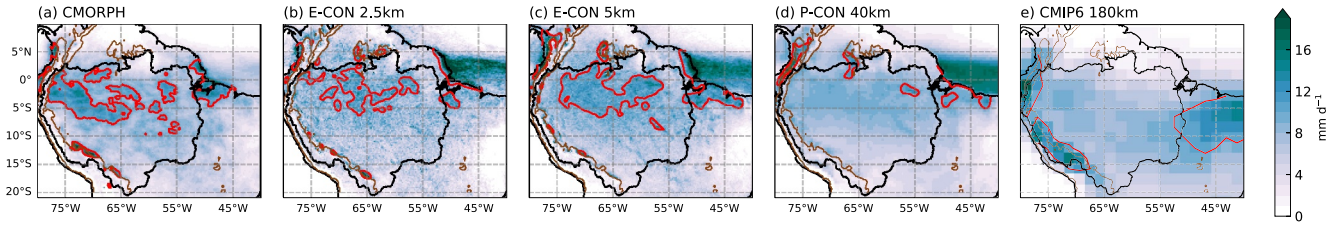

Figure 1. Mean precipitation rate (mm d^{-1}) in March from (a) CMORPH observations, simulations with explicit (E-CON) convection at (b) 2.5 km, (c) 5 km, parameterized convection (P-CON) at (d) 40 km and the (e) CMIP6 multi-model ensemble mean. Only the E-CON ensembles are regrided to CMORPH resolution. Red contours indicate land precipitation rate of 10 mm d^{-1}. The Amazon basin is defined as black contours and the topography at 1,000 m, in brown contours.

35°S–35°N) to 10 km (90°W–30°E, 30°S–30°N) and to 5 km (85°W–25°E; 25°S–25°N), with the finest grid spacing covering the tropical Atlantic sector. In all domains the vertical resolution includes 90 levels, with the model top at 75 km.

We performed eight stand-alone simulations, in which no data was assimilated into the model after initialization. Each member starts on different days at the beginning of March representing different atmospheric states. Given that we prescribe the same time-invariant sea surface temperature (SST), the simulation members aim to account for internal variability arising from the atmosphere alone. The imposed SST is a climatology of the boreal spring season (March–April–May, MAM) from 1950 to 2013. The initial experimental design envisioned the simulations for 3 months but to increase the ensemble size we decided to limit the simulated time to 40 days. Differences in the climatology period (1950–2013) with respect to the observed precipitation (2010–2019) are more associated with differences in the SSTs (March vs. MAM) than with the different periods (1950–2013 vs. 2010–2019). This gives rise to a warmer northern hemisphere than what is seen in March. The impact of, what in retrospective was a sub-optimal experimental design, is discussed in Section 3.1.

We conduct another set of simulations using an updated version of ICON (v2.6.01) with an additional inner domain, at a grid spacing of 2.5 km, that bounds the region: 81°W–36°W; 21°S–11°N. Given the high computational demands, only 2-member simulations are performed considering the two first cases of the 5 km configuration.

In our analysis we compare the 8-member ensemble of P-CON and E-CON at 40 and 5 km, respectively, with the 2-member ensemble of E-CON at 2.5 km. Although from different ensembles, the E-CON simulations at 2.5 and 5 km lead to the same results as those E-CON at 2.5 and 5 km from the 2-member ensemble. We present the results of the 8-member E-CON simulations at 5 km due to more robust statistics. In all cases, the analysis is performed over the last 31 days.

For all quantitative analysis observed data and simulation outputs are regrided to P-CON resolution unless otherwise specified. Interpolating the E-CON simulations to different coarse grids (P-CON, CMORPH) do not affect the results. For the purpose of visualization, however, map figures show the E-CON simulations with the same resolution of CMORPH.

3. Representation of Precipitation

3.1. Geographic Distribution

One of the basic metrics when evaluating the representation of rainfall is the mean amount of precipitation, and its spatial pattern. The prevailing bias in most climate models is the underestimation of rain in the Amazon, especially during the wet season (Fiedler et al., 2020). Spatially, the bias shows up as enhanced rain over the eastern region of Brazil and insufficient rain in the central Amazon (Figure 1e). This southward shift of the ITCZ does not appear to be related to a poor representation of SST patterns in coupled models, but to a westerly wind bias as it has been documented in simulations using prescribed SST (Richter & Xie, 2008).

Both E-CON and P-CON display a better representation of the mean spatial pattern, meaning more rain over the central Amazon and less over eastern Brazil in contrast to the CMIP6 ensemble (Figures 1b–1d). However, two main discrepancies are identified between the E-CON and P-CON simulations and the CMORPH dataset. These discrepancies can be explained by the fixed SST pattern used in the simulations, which results in an artificially

Table 1
Averaged Precipitation Rate (mm d^{-1}) Over the Amazon Basin (AB) Excluding Regions Were Topography Is Above 1,000 m and the Ratio of Amazon and Tropical South America (SA, 20°S–10°N; 80°W–38°W) Rain Rates

Data set	Mean precipitation rate AB (mm d^{-1})	Ratio AB/SA
CMORPH	8.07 (7.86)	1.28
E-CON 2.5 km	7.88 (7.71)	1.21
E-CON 5 km	8.42 (8.19)	1.19
P-CON 40 km	7.52 (7.33)	1.17
CMIP6 180 km	7.41 (7.82)	1.08

Note. Values in parentheses are the averages considering also high topography. For these calculations, CMORPH and output simulations were spatially interpolated onto the CMIP6 grid (180 km).

warmer northern tropical Atlantic than observed (see Section 2.3.1). First, given the invariant warm SST north of the equator, both E-CON and P-CON strongly overestimate ocean precipitation off the Brazilian coast. Second, the simulated land precipitation band is also enhanced north of the Amazon basin. As a result, the E-CON and P-CON simulations displayed less precipitation than the CMORPH dataset south of 5°S and over eastern Brazil (see also Figure S1 in Supporting Information S1). Despite the limitation of the fixed SST pattern used in the simulations, it is still worthwhile to make the comparison with observed precipitation, also considering that E-CON and P-CON have the same conditions. For instance, in the case of the P-CON ensemble, the spatial distribution is more uniform, with no regions having precipitation rates larger than 10 mm d^{-1} (see red contours in Figure 1). The E-CON ensembles do show sub-regions with larger mean values in the central Amazon and similar to CMORPH, but rainfall over parts of the western Amazon is still underestimated (Figure S1 in Supporting Information S1). This characteristic appears insensitive to modest changes in the grid spacing, as evidenced by the similarity between the 2.5 and 5 km E-CON ensembles (Figures 1b and 1c).

A more localized feature, which appears to be sensitive to the treatment of convection, is the coastal precipitation over the northeastern coast of Brazil. Simulations with parameterized convection (P-CON and CMIP6) show a lack of precipitation in this region, a bias that is not evident in the E-CON ensembles. Even with the same SST conditions P-CON partitions precipitation between ocean and inland coast north of 0°, whereas E-CON displays continuous enhanced precipitation also over coastal land. Considering the warmer SSTs and greater ocean precipitation in E-CON than is observed (as discussed in the previous section), the overestimation of coastal ocean precipitation as compared to CMORPH is not surprising. What distinguishes the E-CON ensembles is the ability to simulate coastal precipitation over land, something believed to be important also for precipitation over the Amazon (e.g., Greco et al., 1990). Improvements in the representation of coastal precipitation over land with explicit convection might be related to a better representation of sea-breeze circulations and/or the transition from shallow to deep convection as it will be discussed in Section 3.3.

A quantitative comparison is presented in Table 1. Precipitation is averaged over the Amazon basin, considering the boundaries shown in Figure 1 (Lehner et al., 2006), and the continental region comprised by 20°S–10°N; 80°W–38°W. Even though the differences among simulations are relatively small (<1 mm d^{-1}), this analysis suggests that the E-CON simulations better match the observed precipitation in regions of less orographic relief (regions below 1,000 m above sea-level) and increasingly so with finer grid spacing. When considering regions with elevated topography, CMIP6 shows the closest value to CMORPH; however, this is only due to the excessive precipitation over the Andes, which can be related to the poor representation of topography at such coarse resolutions (e.g., Gao et al., 2006). Regarding our simulations, both E-CON ensembles differ from observed values by less than 0.35 mm d^{-1} while precipitation biases of the P-CON simulations are nearly twice as large (>0.5 mm d^{-1}).

Comparing the ratio between Amazon precipitation and the tropical continent as a whole, both E-CON and P-CON display a ratio of about 1.2, similar to what is observed, whereas the CMIP6 ensemble shows a value closer to 1. This is again related to the enhanced precipitation over high topography and over the eastern coast of Brazil in the CMIP6 ensemble. Although the improvements are small, the most highly resolved E-CON simulations are overall the closest to CMORPH.

Some aspects of the simulations show less indication of improving with a reduction of the grid spacing at storm-resolving scales. While all simulations with explicit convection do a fair representation, one might expect a better performance for the 2.5 km mesh simulations as compared to those with a 5 km mesh. For instance, along the eastern flank of the Andes (from 10°S–17°S; Figure 1), the Amazon comprises some of the rainiest places in the region, exhibiting features known as "precipitation hot spots" (e.g., Chavez & Takahashi, 2017). The E-CON ensembles exhibit a similar zonal gradient that maximizes eastward; however not as prominently as is seen in CMORPH. Although the enhancement of precipitation north of the Amazon may contribute to the decreased precipitation east of the Andes, the similarity between the 2.5 and 5 km ensembles suggests that other

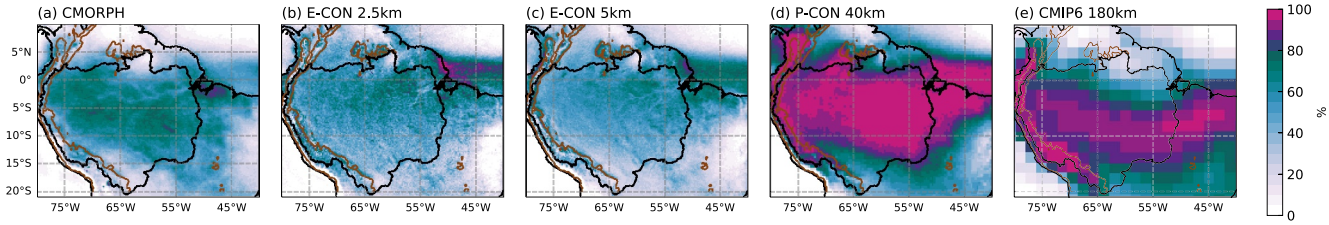

Figure 2. Frequency (%) of daily precipitation rate greater than 1 mm d^{-1} in March from (a) CMORPH data and simulations with explicit (E-CON) convection at (b) 2.5 km, (c) 5 km, parameterized convection (P-CON) at (d) 40 km and the (e) CMIP6 multi-model ensemble mean. Only the E-CON ensembles are regrided to CMORPH resolution. The Amazon basin is defined as black contours and the topography at 1,000 m, in brown contours.

unresolved processes might as well be at play. For instance, resolving yet smaller scale orographic features could improve daytime precipitation through thermally driven circulations in mountain ridges and embedded valleys (Junquas et al., 2018). Also, changes in the microphysical parameterization would influence the representation of stratiform rain of these precipitation hot spots, which occurs preferably overnight (Chavez & Takahashi, 2017).

Overall, improvements in the representation of the mean precipitation are not remarkable. The IFS convective parameterization used in the P-CON ensemble sets a high bar. It shows a better geographic distribution than average climate models (i.e., CMIP6) and clear improvements from the use of E-CON are only apparent in specific features.

3.2. Frequency and Intensity

The E-CON ensembles show a notable improvement in the estimated frequency and distribution of precipitation intensity in the Amazon basin (Figure 2). The frequency of daily precipitation follows the spatial pattern of the mean precipitation (Figure 1), featuring regions where it rains up to 80% of the days in E-CON and CMORPH (Figures 2a–2c). The E-CON ensembles also distinguish more rain frequency over land areas than rivers, such as the Amazon river mouth and the Tapajos river (Figures 2b and 2c), although details are smoothed due to the interpolation to the common analysis grid.

A very different picture is displayed by simulations with parameterized convection, as P-CON shares the biases of the CMIP models, which tend to overestimate the frequency of light rain (Stephens et al., 2010) regardless of the spatial resolution (Figures 2d and 2e). Regions where the mean precipitation is greater or equal than 5 mm d^{-1} (Figure 1) show a frequency greater than 90%–95%, indicating that the mean precipitation amount is related to the persistence of rainy days.

To have a broader view of the frequency spectra, Figure 3 displays the distribution of precipitation intensity over the Amazon basin. The E-CON ensembles show an important improvement in the representation of this

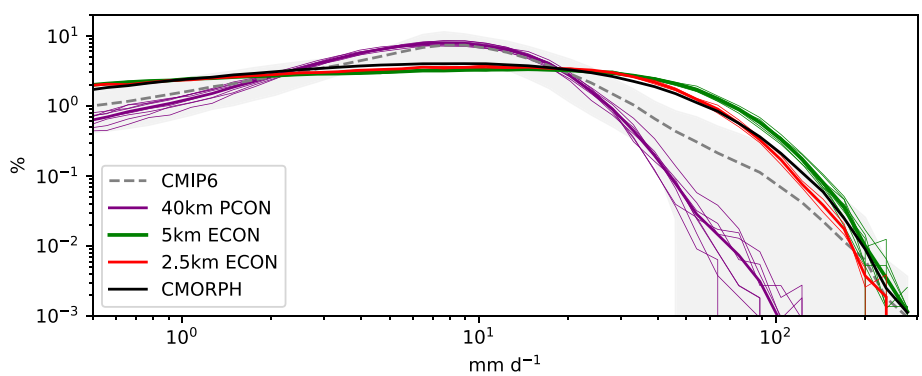

Figure 3. Distribution (%) of daily precipitation intensity greater than 0 mm over the Amazon basin for CMORPH data (black line) and simulations (colored lines). Values are binned in a logarithmic scale. The gray shading represents the standard deviation of 14-models of the CMIP6 ensemble. Thinner contours represent each member of E-CON and P-CON ensembles.

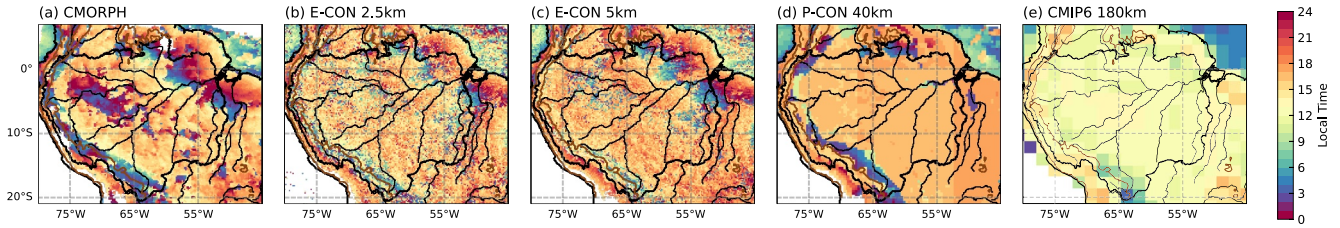

Figure 4. Local time (hour) of maximum precipitation in (a) CMORPH data and simulations with explicit (E-CON) convection at (b) 2.5 km, (c) 5 km, parameterized convection (P-CON) at (d) 40 km and the (e) CMIP6 multi-model ensemble mean. Only the E-CON ensembles are regrided to CMORPH resolution. In all cases, the hourly mean was calculated and smoothed using a second order Fourier transform per grid point. The Amazon basin is defined as black contours as well as the rivers (thinner contours), and the topography at 1,000 m is shown in brown contours.

precipitation feature as compared to simulations with parameterized convection and in agreement with studies focused on different regions (e.g., Becker et al., 2021; Holloway et al., 2012; Judt & Rios-Berrios, 2021). This improvement is evident across the E-CON ensembles, which suggests that it is determined by the treatment of convection rather than the details of the spatial resolution and the experimental set-up (global vs. nested, not shown). In a recent comparison study, Judt and Rios-Berrios (2021) showed that simulations with full convective parameterization run at about 4 km grid spacing displayed the same distribution of precipitation intensity as those at 100 km.

Differences in the intensity spectrum are most evident in two intensity intervals. First, the interval between 2 mm d^{-1} to 20 mm d^{-1} (light-to-moderate rain) occurs more frequently, with a clearly preferred intensity in simulations with parameterized convection. CMORPH and the E-CON ensembles show a flatter distribution, and less frequent rainfall in this intensity interval as a whole. The second intensity interval covers precipitation rates greater than 25 mm d^{-1} (high intensity rain). As compared to CMORPH and to E-CON, these high-intensity rain events are much rarer in P-CON. The inter-model variability in the representation of intense precipitation is large across the CMIP6 models, showing a larger frequency of the multi-model ensemble mean than the P-CON ensemble but still below what is observed. Considering individual CMIP6 models, two out of 14 are close to E-CON and CMORPH and one overestimates frequencies larger than 100 mm d^{-1}. This suggests that use of convective parameterization does not seem to necessarily preclude a reasonable representation of extreme rainfall over the Amazon. For intervals that account most of the total precipitation spectra (light-to-moderate rain), the persistence of the too frequent and too gentle bias (Fiedler et al., 2020; Judt & Rios-Berrios, 2021; Stephens et al., 2010) in all simulations employing parameterized convection suggests that it is not easily addressed in the framework of existing convective parameterizations. The considerably better agreement between CMORPH data and simulations that represent convection explicitly, suggests that linking precipitation development to convective motion fields places physical and meaningful constraints on the intensity distribution in ways that parameterizations of convection are unable to mimic.

3.3. Diurnal Cycle

The diurnal cycle of precipitation over the Amazon is not spatially homogeneous. To illustrate this feature, we compute the hourly mean for each grid point and then select the time when precipitation is maximum (Figure 4). This method allows us to consider semidiurnal variations and avoid ambiguities that arise when using the first harmonic approach (Yang et al., 2008).

A large part of the Amazon basin depicts a precipitation maximum in the afternoon from 15 to 18 Local Time (LT) as a result from daytime heating. The afternoon peak is reasonably well represented by E-CON and P-CON simulations, although in the case of P-CON, elements of the parameterization were specifically designed to capture this effect (Bechtold et al., 2008). Nonetheless, it shows that such delays can be represented in the framework of convective parameterization, and thus constitutes an important improvement, but one that apparently has yet to find its way to the CMIP6 multi-model ensemble (Figure 4e), as these models still tend to precipitate too early (Fiedler et al., 2020; Tang et al., 2021).

Perhaps due to the way in which it was implemented, the P-CON simulations displays a rather homogeneous spatial distribution of the time of maximum precipitation. The E-CON simulations, on the contrary, can

reproduce observed spatial heterogeneities in the diurnal cycle naturally. The time of diurnal precipitation maxima varies between 15LT and 18LT, albeit the 5 km E-CON ensemble displays predominantly a peak time closer to 18LT in contrast to the 2.5 km ensemble. The earlier precipitation peaks in the afternoon with finer grid spacings in explicit convection simulations has been also found in previous studies (e.g., Sato et al., 2009; Yashiro et al., 2016). Yashiro et al. (2016) suggests that grid spacings less than 2–3 km can reproduce weak convection with precipitation in the late morning; whereas the coarser the grid spacing, the more energy it is required to trigger grid-scale convection near the surface and thus peaking precipitation times occur later in the day.

The spatial heterogeneity of the diurnal cycle in the E-CON ensemble shows a structure that is also evident in CMORPH. Notable in this respect is the consecutive peaking times from the northeast coast moving inland toward the Amazon. Near the coast, precipitation maximizes close to midday (12-14LT), a feature that may be related to relatively shallow and unorganized convection (e.g., Houze Jr et al., 2015). Precipitation maximizing later in the day, increasingly so as one moves inland, agrees with what would be expected from transition to deep convection that propagates toward the Amazon (Burleyson et al., 2016; Greco et al., 1990). The representation of such progressive peaking times and corresponding increasing cloud depth (not shown) suggest that the E-CON ensembles are able to reproduce a realistic transition of convection.

Notwithstanding the general tendency of precipitation to maximize during the day, there are places where precipitation peaks overnight (Garreaud & Wallace, 1997; Janowiak et al., 2005; Rickenbach, 2004; Tanaka et al., 2014). Apart from nocturnal precipitation placed east of the Andes, two regions stand out in CMORPH data displaying a horse-shoe pattern between 75°W–65°W and 60°W–50°W at 10°S–0° (Figure 4a). This structure is captured by the E-CON ensembles (Figures 4b and 4c) but is not observed in P-CON or CMIP6. For instance, the northeast extreme of the Amazon basin exhibits a coast-parallel band of consecutive peaking times from 21LT to 6LT (Figures 4a–4c). This nocturnal precipitation band has been associated with squall lines, which can originate at the coast and move inland (e.g., Garstang et al., 1994). The second region displaying nocturnal precipitation peaks is not as pronounced in the E-CON ensembles as in CMORPH, but still can be distinguished inland between 65°W–75°W, 5°S–0°. This discrepancy could be attributed to the interannual variability captured by the CMORPH climatology in contrast to our simulations and to less OCS simulated over that region by E-CON compared to CMORPH (see next section). Moreover, many of the nocturnal precipitation peaks also co-locate with the Amazon river and its tributaries, suggesting a sensitivity to the representation of thermally-driven local circulations (e.g., Fitzjarrald et al., 2008; Tanaka et al., 2014; Wu et al., 2021).

Over the eastern flank of the Andes, particularly south of 10°S, a nocturnal peak in precipitation is apparently better captured by P-CON than E-CON ensembles. Closer inspection shows an eastward misplacement of these systems in P-CON, locating the nocturnal peaks toward the Amazonian plains. The E-CON ensembles display a more similar location of this nocturnal band over the Amazon-Andes transition as seen CMORPH, increasingly so as the grid is refined but still not as pronounced as in CMORPH. As discussed in Section 3.1, precipitation over the eastern flank of the Andes is associated with stratiform features, especially during night (Chavez & Takahashi, 2017). The modest improvement by the 2.5 km ensemble shows again that a twofold refinement of the grid spacing does not guarantee a correct performance of the simulated diurnal cycle in the Amazon-Andes transition. Thus, cloud microphysics could have a greater impact on representing the nocturnal peaks related to stratiform rain over this region.

In terms of the amplitude of the precipitation diurnal cycle, Figure 5 shows that both E-CON ensembles particularly overestimate precipitation associated with deep convection during the afternoon (at about 15-17LT), whereas the P-CON ensemble shows a closer amplitude to CMORPH. Moreover, in contrast to the results of Inoue et al. (2021), the secondary peak in the early morning is slightly underestimated and rather delayed by 3 hr in both E-CON ensembles. Considering that the secondary peak might be more related to stratiform rain, this misrepresentation could be associated with the reduced nocturnal precipitation peaks by E-CON (Figure 4). There are not considerable differences between the 2.5 and 5 km ensembles regarding the amplitude, but only in the phase as discussed above. As for P-CON, the secondary peak is not clear given its rather flat curve, albeit its amplitude is closer to CMORPH between 0-4LT.

Hence, the IFS convection scheme used by P-CON can overall capture the amplitude of the diurnal cycle, to some extent better than E-CON. However, its inability to capture the spatial variations in the phasing of precipitation as well as E-CON suggests that the reason of such improvement may be more a result of fitting than of physical constraints.

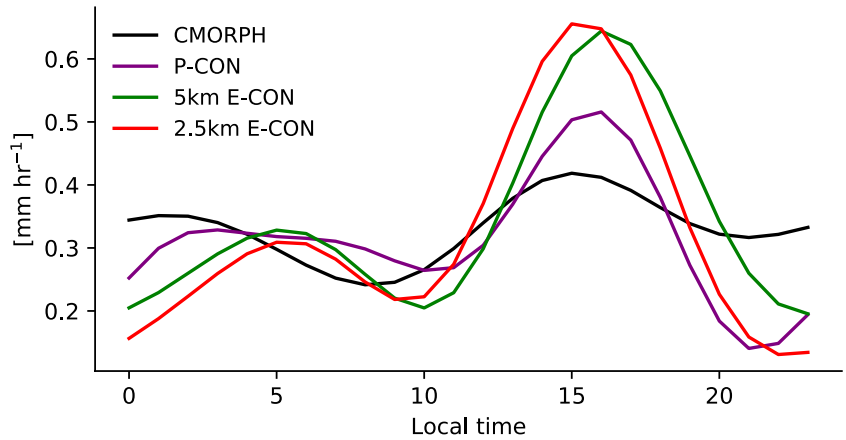

Figure 5. Diurnal precipitation rate (mm d^{-1}) averaged over the Amazon basin.

4. Role of Organized Convective Systems

In Section 3 we compared some precipitation characteristics between observations and small ensembles of simulations, differing in their treatment of convection and in their spatial resolution. An explicit representation of convective precipitation is shown to improve the representation of Amazon precipitation, most notably in terms of the distribution of precipitation intensity and the spatial heterogeneity of the diurnal cycle. These precipitation characteristics can be related to OCS, which develop during the day and can last overnight generating very intense rainfall episodes (e.g., Garreaud & Wallace, 1997; Pereira Filho et al., 2015; Rehbein et al., 2018; Rickenbach, 2004).

In this section we analyze whether improvements in the representation of the precipitation intensity and diurnal cycle by the E-CON ensembles are related to the representation of OCS in the Amazon. Considering that simulations with parameterized convection fail in reproducing such precipitation features (i.e., high intensity rain rates and heterogeneity in the diurnal precipitation peaks), we mostly focus the analysis on the E-CON ensembles.

In the following subsections we examine precipitation characteristics of precipitation objects and compare them with the non-organized precipitation. To define precipitation objects, or what we call OCS we use an object-based approach. First, precipitation is associated with grid cells whose hourly rain rate is equal to or greater than 2 mm hr^{-1}. Precipitation objects are then identified as contiguous grid cells (8-way connection) with a minimum size of 10,000 km^2 (equivalent to six grid cells on the coarsened analysis grid) at each hour. Given that we do not track the OCS, this method preferentially samples mature systems. Therefore we chose a size threshold similar to the mean size found in past studies (Anselmo et al., 2021; Rehbein et al., 2018), which are about 14,000 km^2 (based on brightness temperature). Even so, we test our findings by redoing the analysis using different thresholds and this did not change our findings.

4.1. Frequency of Intensity and Size

Figure 6a shows the distribution of precipitation intensity of OCS only (solid lines) and non-organized precipitation (dashed lines). By comparing Figure 6a with Figure 3 one can notice a better agreement between the E-CON ensembles and CMORPH data when only considering the OCS. In particular, the 5 km ensemble fits well the observed frequencies between 10 mm d^{-1} to 200 mm d^{-1}.

Precipitation associated with OCS explains the high-intensity rates (>100 mm d^{-1}) in the observed dataset. The distribution of non-organized precipitation in CMORPH resembles the P-CON distribution related to OCS and that in Figure 3 (purple line). In contrast, non-organized precipitation in the E-CON ensembles still shows larger frequencies of intense rain (around 200 mm d^{-1}). This shows a tendency of the E-CON simulations to produce more intense isolated events, a deficiency that has also been noted by previous studies in kilometer-scale simulations (Arnold et al., 2020; Prein et al., 2015).

The relative contribution of OCS to the total rainfall can be associated with the distributions of precipitation intensity. In observations, most of the intense precipitation (>50 mm d^{-1}) is associated with OCS (e.g., Feng

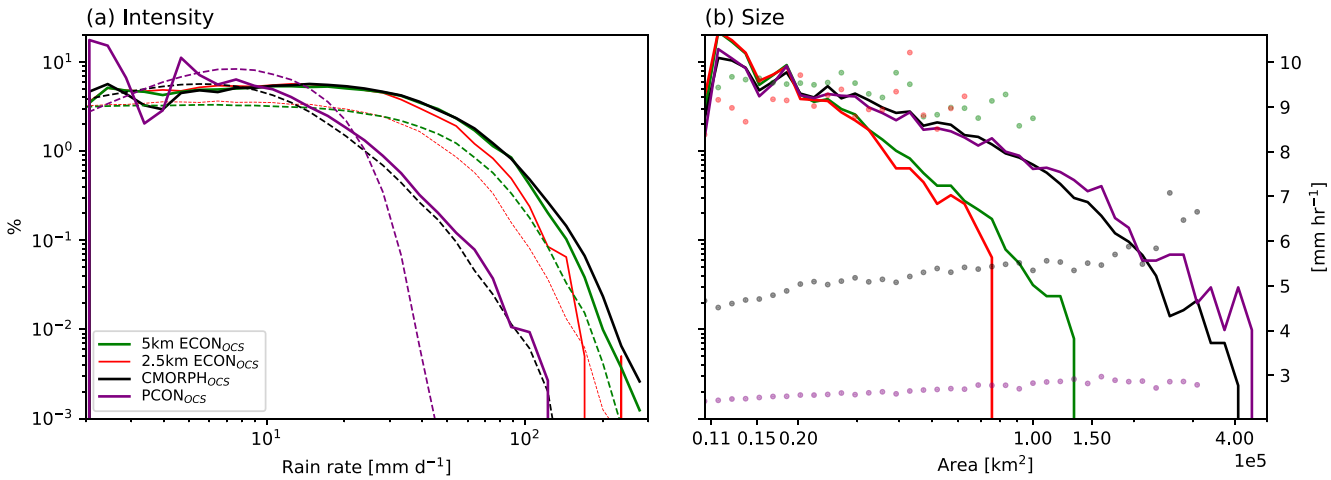

Figure 6. (a) Distribution (%) of daily precipitation intensity of organized convective systems (OCS, solid lines) and non-organized precipitation (dashed lines) in the Amazon basin. (b) Size distribution of organized convective systems (solid lines) and mean precipitation per area bin (scatter points, right axis). CMORPH is displayed in black, the E-CON ensembles in green (5 km) and red (2.5 km) colors and the P-CON ensembles in purple. Values of intensity and size are binned in a logarithmic scale.

et al., 2021). The contribution of OCS in the E-CON ensembles is not as large as observed (30% in the simulations as compared to about 50% in the observations, not shown). This might be related to the overall underrepresentation of the size of OCS in the simulations (Figure 6b). As found in some previous studies (e.g., Arnold et al., 2020; Crook et al., 2019), the storm-resolving simulations generally produce smaller precipitation clusters than those identified in CMORPH. The median size for 5 and 2.5 km E-CON ensembles are 14,411 km^2 and 14,371 km^2, respectively; whereas for CMORPH it is 19,224 km^2. Likewise, the median intensity per bin size is about twice in E-CON than CMORPH (colored dots in Figure 6b). The size distribution of OCS shows that E-CON overestimates the frequency of systems smaller than <20,000 km^2 and misses those larger than 1,50,000 km^2. The size distribution of P-CON looks more closely aligned with the observed dataset. However, it primarily refers to connected precipitating grids which lack the convective signature of OCS, resulting in rain rates that are about half of what is observed.

The large discrepancies of OCS intensity and size between E-CON and CMORPH do not change considerably between 2.5 and 5 km ensembles, meaning that these biases might be associated with unresolved processes (i.e., sub-hectometer scales) such as cloud microphysics. For instance, Feng et al. (2018) found that a better representation of stratiform rain results in a better representation of precipitation area in mesoscale convective systems at storm-resolving resolutions. This suggests that microphysical processes might be important for properly representing some macrophysical properties of OCS in the Amazon (e.g., size).

4.2. Diurnal Cycle

Considering precipitation only from OCS improves the similarity of the spatial structure in the phase of the diurnal cycle between E-CON and observations (Figures 7a–7c). Especially in the western Amazon, precipitation peaks occurring during night and early morning are as apparent in the 5 km E-CON ensemble as in CMORPH. This feature is noisier in the 2.5 km ensemble probably due to the smaller sample size than the 5 km ensemble. In contrast, P-CON OCS are mostly absent in the Amazon basin and disagree with the observed spatial structure.

The OCS explain most of the spatial heterogeneity in the diurnal cycle of observed precipitation (compare Figures 7a, 7d and 4a). This feature is less in evidence in E-CON over the central Amazon, although the reduced frequency of OCS in the E-CON ensembles (about 1580 OCS per member in both E-CON ensembles against 4250 OCS per year in CMORPH) may explain the difference with CMORPH. While there are clear regions of nocturnal precipitation maximum in the simulated OCS, they are delayed by a few hours as compared to what is observed. CMORPH displays a nocturnal peak preferably between midnight and 3LT, whereas peaks between 3LT to 6LT are more apparent in the 5 km E-CON ensemble. This delay is also seen in the diurnal variation of the size of OCS, in which the largest OCS in E-CON peak few hours after the observed peak (Figure S2 in Supporting

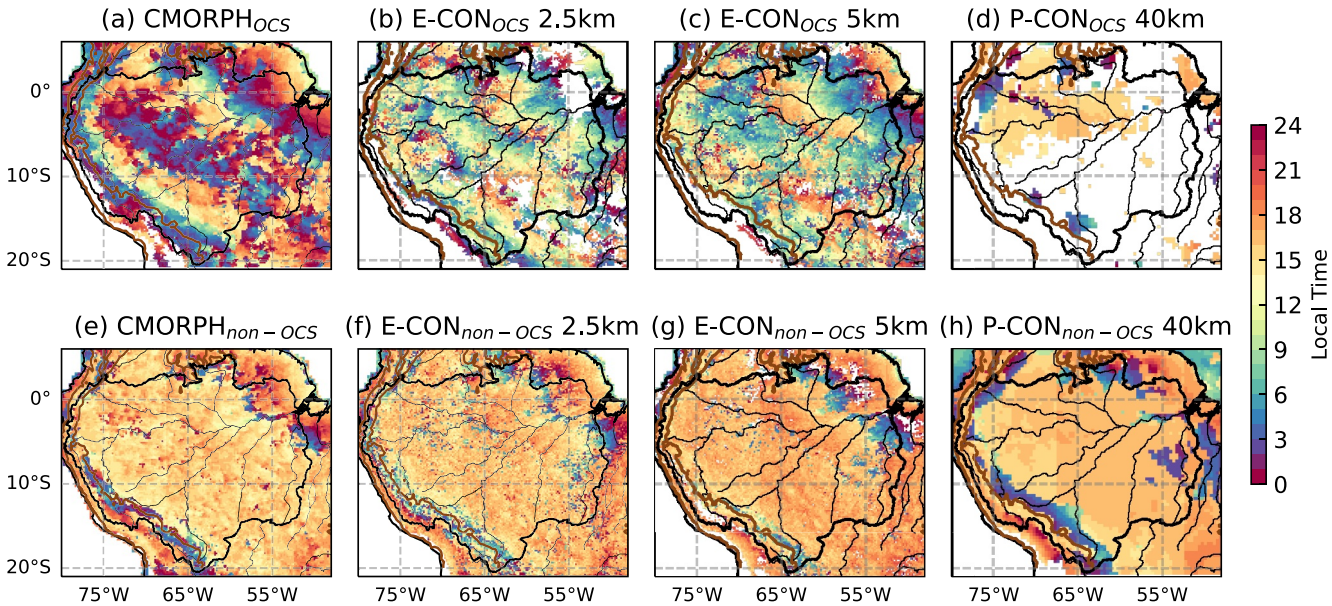

Figure 7. Local time (hour) of maximum precipitation (a, b, c, d) considering only organized convective systems (OCS) and (e, f, g, h) only non-organized precipitation (*"non-OCS"*) for (a), (d) CMORPH, (b), (e) 5 km E-CON (c), (f) 2.5 km E-CON simulations and (d), (h) P-CON. For the purpose of this figure, the identification of OCS considered regions outside the Amazon. Only the E-CON ensembles are regrided to CMORPH resolution. The Amazon basin is defined as black contours as well as the rivers (thinner contours), and the topography at 1,000 m is shown in brown contours.

Information S1). Regarding the diurnal peaks (12LT to 18LT), these are more similar between CMORPH and E-CON, especially at 2.5 km. Other features associated with the diurnal cycle of OCS by E-CON are also consistent with CMORPH. For instance, the most intense and smaller OCS occur in the late afternoon in agreement with their mature phase, whereas the opposite conditions take place in the early morning, consistent with a decay stage of these systems (Houze Jr, 2004) (Figure S2 in Supporting Information S1).

Non-organized precipitation features daytime precipitation maximum ranging mostly from 12LT to 18LT (Figures 7d–7f), with predominantly peaking times at about 15LT in CMORPH, at 16LT in 2.5 km E-CON and P-CON, and at 18LT in the 5 km E-CON ensemble. Despite the overall diurnal peaks some regions display maximum precipitation overnight. For instance, scattered nocturnal peaks in the central Amazon in CMORPH and the E-CON ensembles, probably associated with very intense rain rates from isolated convective cells (Figure 6a), are placed near the Amazon river and its tributaries.

While diurnal precipitation peaks seem to improve with increased resolution (Sato et al., 2009), especially for non-organized precipitation, nocturnal precipitation peaks associated with OCS remain similar between 2.5 and 5 km ensembles. Other features such as the intensity and size of OCS are also more similar between the two E-CON ensembles than as compared to CMORPH, suggesting no systematic improvement with a twofold refinement of the grid spacing. This insensitivity to spatial resolution might indicate once more that other unresolved processes are important for further improving the representation of the OCS life cyle in the Amazon, especially those contributing to nocturnal stratiform features (Houze Jr, 2004). Notwithstanding the above-mentioned differences between E-CON and CMORPH, the results show unique properties of Amazon precipitation (distribution of precipitation intensity and spatial heterogeneity in the diurnal cycle) are due to the presence of OCS which, although still in a coarse form, are captured by both E-CON ensembles.

5. Environmental Conditions Related to OCS

5.1. Classification of OCS

To better understand the structure of the simulated OCS and environmental factors that influence them, we objectively identify the main types of OCS by applying the k-means clustering technique to their computed statistics: time of occurrence, size, intensity and location (defined as the center of gravity of each, weighted by precipitation) within the whole Amazon basin. We also use the Silhouette score (Rousseeuw, 1987), which finds

Table 2
Summary of Clusters Features in the 5 km E-CON Ensemble and CMORPH (in Parentheses)

Cluster	Local hour	Intensity (mm h^{-1})	Area (km^2)	Latitude	Longitude	Fraction (%)
D1	17 (18)	9.8 (4.9)	15,513.2 (21,742.6)	−2.8 (−9.0)	−64.1 (−60.6)	20.8 (22.9)
D2	12 (13)	9.0 (4.7)	15,561.69 (22,901.6)	−12.3 (−2.9)	−65.5 (−72.0)	16.3 (25.5)
D3	13 (13)	17.3 (8.8)	15,048.7 (25,949.4)	−5.7 (−5.2)	−65.9 (−67.1)	12.3 (10.0)
N1	6 (7)	9.0 (4.8)	16,671.1 (24,898.3)	−3.7 (−3.2)	−58.1 (−58.4)	22.6 (17.8)
N2	8 (5)	8.6 (4.8)	16,793.1 (23,447.9)	−3.4 (−11.5)	−72.6 (−65.5)	22.6 (17.5)
N3	9 (10)	9.4 (5.7)	47,832.2 (102,669.8)	−5.8 (−5.6)	−67.4 (−66.3)	5.4 (6.4)

Note. The median values are presented for the local hour, intensity, area and location (latitude and longitude). The last column indicates the fraction that a given cluster represents from the total number of OCS (27883 in E-CON and in 43054 CMORPH).

the optimum number of clusters based on a measure of cluster cohesion and separation. The analysis is focused on the 5 km E-CON ensemble considering its overall similarity with the 2.5 km ensemble and given its larger sample size. CMORPH data serve only for comparison of the OCS classification.

Six OCS clusters are identified in both E-CON and CMORPH (Table 2, Figure S3 in Supporting Information S1). Among these, a clear distinction is associated with their time of occurrence rather than their size or intensity. Given that OCS represent mature systems, we refer to those that occur in the afternoon (12–18 hr) as diurnal (D1, D2, D3), and to those that occur in early morning (5–10 hr) as nocturnal (N1, N2, N3) OCS. Each of them accounts for about 50% of the total OCS in E-CON (49.4% for diurnal and 50.6% for nocturnal); whereas in CMORPH, diurnal OCS are more clearly favored (58.4% vs. 41.6%).

Other common features between E-CON and CMORPH OCS are found in clusters N1, N3 and D3. The N1-OCS distinguish from other nocturnal OCS because of their center of gravity is placed in the northeast Amazon (Figure S3 in Supporting Information S1), which would correspond to the well-known squall lines propagating from the coast (e.g., Garstang et al., 1994). N3 and D3 OCS do not show a preferred location of occurrence but they are characterized by their large size and high intensity, respectively.

Contrasting the remaining OCS (N2, D1, and D2) between E-CON and CMORPH, these mainly differ in their center of gravity and are more symmetrically distributed in the simulations than in the observed data (Figure S3 in Supporting Information S1). For instance, D1-OCS and D2-OCS comprise the northern and southern Amazon in the E-CON ensemble, respectively; whereas D2-OCS only cover the northwestern Amazon and D1-OCS, the rest of the basin in CMORPH. As opposed to N1-OCS, N2-OCS comprise the northwestern Amazon in E-CON; but they cover a large region in the southern Amazon in CMORPH.

Apart from differences in the location of three clusters of OCS, other features are consistent between E-CON and CMORPH. Albeit with differences in magnitude as discussed in Section 4.1, both intensity and size follow the expected life cycle of OCS. Diurnal clusters are characterized by overall most intense but not too large OCS, whereas nocturnal clusters feature the largest and overall less intense OCS. Considering this important similarity, we conclude that the E-CON ensemble makes a fair representation of the observed classification of OCS.

5.2. Influence of the Environment on OCS Evolution

We further explore the mean environmental conditions as simulated by the E-CON ensemble associated with OCS during their evolution by analyzing composites at different lead and lag times. The purpose of this section is to provide insights on how the more physically-driven E-CON simulations represent the interaction of organized convection and its environment, which could in principle be tested by observations. To simplify the analysis we isolate diurnal and nocturnal events as defined in the previous section (see Table 2). Considering that the 3D field only has 3-hourly output, OCS clusters identified from 12LT are considered diurnal OCS and those occurring before 10LT, nocturnal OCS.

Diurnal and nocturnal OCS show clear distinctions in their vertical structure (Figure 8), with some variations among clusters. For instance, diurnal OCS persist less than the nocturnal OCS at the place of detection. Both the

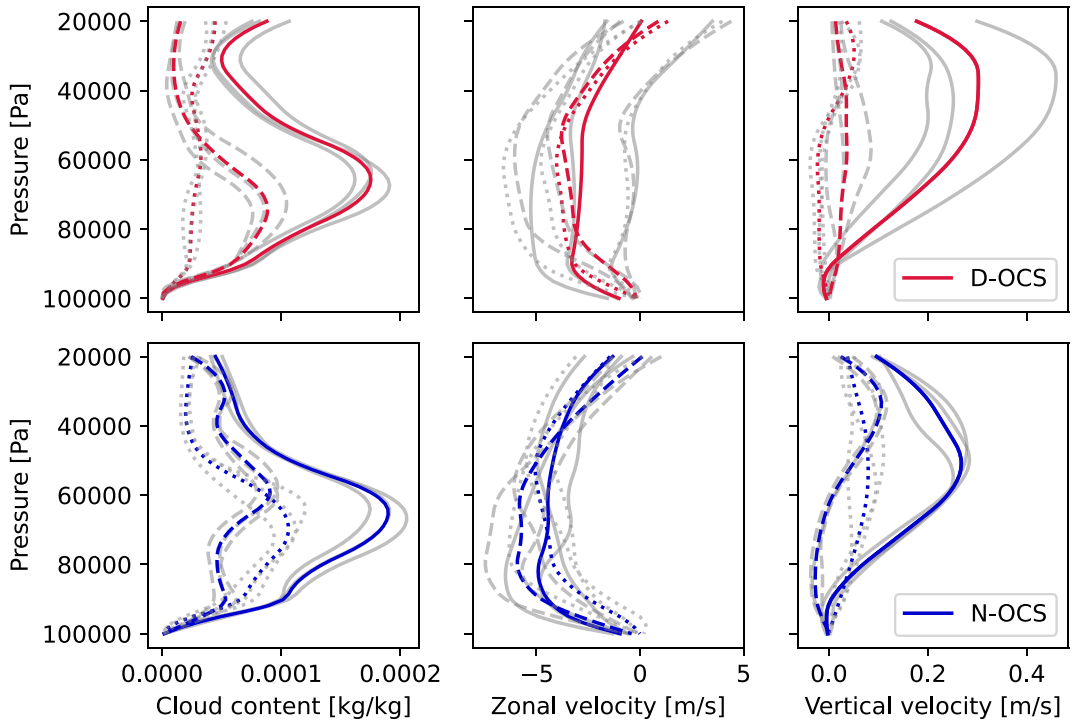

Figure 8. Vertical profile of composite OCS. The variables shown are from left to right: cloud content (water and ice), zonal velocity and vertical velocity. Solid contours represent the vertical profiles at the moment of object detection (time 0), dashed lines represent 3 hr before the detection and dotted lines, 3 hr after time 0. Diurnal (D-OCS) and nocturnal (N-OCS) OCS are located in the upper and lower row, respectively. Gray contours represent the original clusters (D1, D2, D3, N1, N2, N3). The vertical profiles are taken at the center of gravity of the respective OCS, averaged by group and then smoothed using a second order polynomial interpolation.

cloud content and vertical velocity are considerably reduced at 3-hr lead in the diurnal OCS (Figure 8, dotted lines), whereas nocturnal OCS show larger cloud content and vertical velocity from the freezing level (500 hPa) compared to the lower troposphere. This vertical structure suggests persistent and less intense precipitation in the nocturnal OCS consistent with stratiform features, an essential component of mature OCS (Houze Jr, 2004). In contrast, diurnal OCS display enhanced convective activity (i.e., vertical ascent) only at the time of OCS detection, which can be related to a shorter life span or faster propagation than the nocturnal OCS.

The diurnal OCS are associated with a strong (2 K) depression of the surface potential temperature relative to the environment (Figure 9). This local signal is thought to be related to cold pools as shown in Figure 10. The time of detection of cold pools displays successive times of occurrence from 12LT to 17LT in agreement with the OCS propagation, especially in the northeastern Amazon. Figure 9 shows westward-propagating anomalies of potential temperature which are stronger 3 hr before than after the detection of OCS, in agreement with the occurrence of cold pools mainly during the early afternoon. The westward propagation is consistent with the background zonal flow (Figure 8), which displays easterlies through a deep layer (from 950 hPa to 400 hPa). This propagation is more evident in D1-OCS (northern Amazon) and D3-OCS (most intense OCS), whereas D2-OCS (southern Amazon) show rather a stationary pattern, probably due to their far distance from the trade winds (not shown).

The nocturnal OCS are associated with different large-scale conditions as compared to the diurnal OCS. The zonal wind velocity is considerably larger near 800 hPa (Figure 8) than the surface even 3 hr after the OCS detection, especially for N1-OCS (northeastern Amazon) and N3-OCS (largest OCS). The strong easterlies in the lower troposphere can be indicative of the nocturnal low-level jet (Anselmo et al., 2020), which would act against the stable nocturnal boundary layer to sustain convection overnight (e.g., Houze Jr, 2004). Anselmo et al. (2020) found enhanced occurrence of cloud clusters associated with such nocturnal low-level jet, especially during the early morning (2LT to 8LT) which agrees with our results. Moreover, the potential temperature perturbations show larger anomalies above the surface (850 hPa) during the OCS occurrence (Figure 9). A special case is noted in N3-OCS (not shown), which display broader anomalies of potential temperature that last 3 hr after their

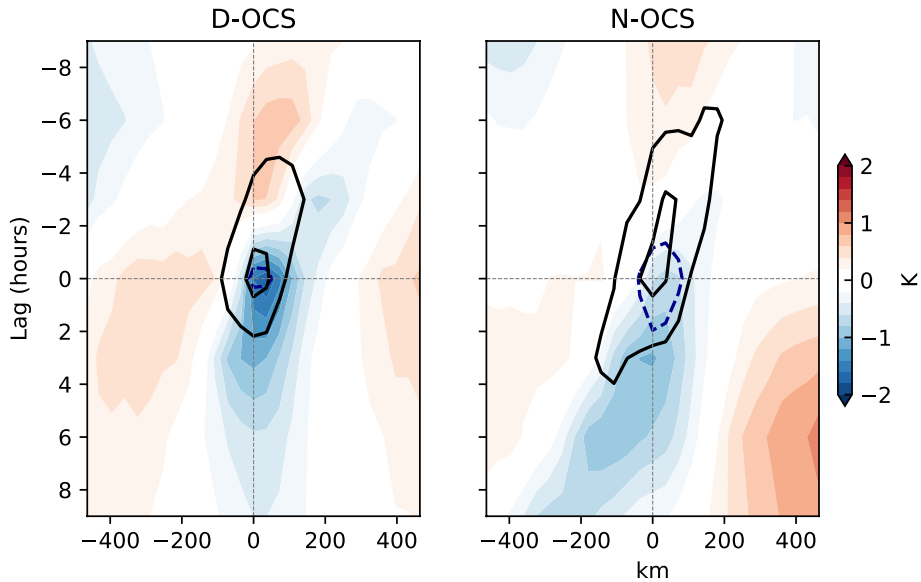

Figure 9. Time-longitude composites of potential temperature perturbations at the surface (1,000 hPa) related to diurnal (left) and nocturnal (right) OCS. Negative anomalies at 850 hPa are shown as dashed-blue contours (−0.3 K). The anomalies (i.e., perturbations) are computed with respect to the zonal mean. Precipitation is displayed as black solid contours (0.2 and 0.5 mm hr^{-1}). Time zero indicates the hour when the OCS are detected and longitude zero is the location of the center of mass of the OCS.

detection. These elevated anomalies might be related to cooling by evaporation of precipitation particles and indicative of their decay stage.

The environmental controls of diurnal and nocturnal OCS as represented by explicitly resolved convection, provide insights of which processes might be important for the temporal phasing and distribution of precipitation. For instance, our results show that the interaction with the surface through the occurrence of cold pools matter mainly for the diurnal OCS, which are underestimated relative to the nocturnal OCS. This suggests that surface processes in relation to deep precipitating convection might need to be better represented at storm-resolving scales, especially considering that OCS tend to originate during the day (Rehbein et al., 2018). Likewise, the overestimation of nocturnal OCS could be the result of favorable large-scale conditions (e.g., strong low-level jet) and possibly inadequate microphysics. Nocturnal OCS display strong cooling and updrafts in the lower troposphere and preserve cloud content at upper levels 3 hr after their detection, indicative of stratiform features. Nonetheless, their sizes are rather small compared to the observed nocturnal OCS. Improving the representation of stratiform rain can also impact the large-scale dynamics in storm-resolving simulations (Feng et al., 2018), which might lead to a better representation of nocturnal OCS.

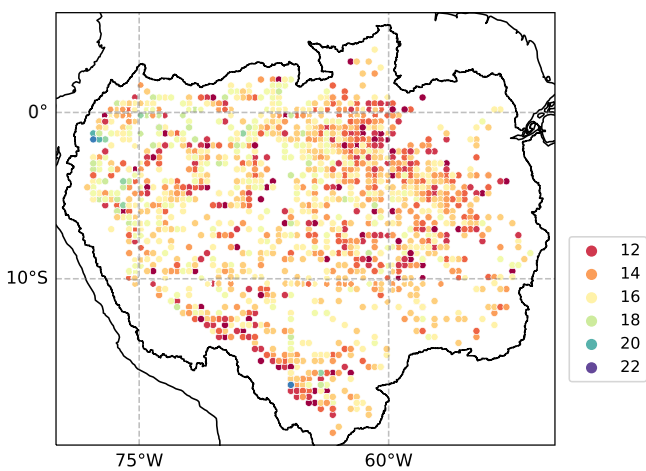

Figure 10. Local hour of cold pool detection during the time of occurrence of OCS. Cold pools are identified considering a potential temperature perturbation larger than −2 K and precipitation greater than 1 mm hr^{-1}, following the approach of Hirt et al. (2020).

6. Summary and Conclusion

This study investigates the ability of storm-resolving simulations to represent precipitating systems over the Amazon river basin. We perform ensemble simulations with the ICON-NWP atmospheric model at a coarse grid spacing (40 km) wherein convection is parameterized (P-CON) and storm-resolving simulations that enable the explicit representation of convection (E-CON) at 2.5 and 5 km grid spacing. The simulations are compared to each other, conventional coarse resolution model output taken from CMIP6, and to observations as represented by the CMPORPH data set.

The mean precipitation in the Amazon basin and its spatial distribution are fairly represented by both E-CON and P-CON ensembles. However, the large

frequency of light rain can explain a close daily mean to observations in the P-CON ensemble. Moreover, P-CON misses precipitation in the northeast land coast which is known to be important for the generation of propagating systems toward the Amazon (e.g., Burleyson et al., 2016; Greco et al., 1990; Rehbein et al., 2018).

Ensembles with grid spacings that allow for explicit convection better represent the distribution of precipitation intensity and the spatial variability of the diurnal cycle, as compared to simulations with parameterized convection. Light-to-moderate precipitation 2 mm d^{-1} to 20 mm d^{-1} and higher intensity rain rates are correctly captured by E-CON; whereas P-CON persists on long-standing biases (e.g., Stephens et al., 2010) as the CMIP models. The spatial heterogeneity (pattern) of the diurnal cycle can also be detected in the E-CON ensemble, similar to what is found in observations. The P-CON ensemble, which is based on one of the best tested and most advanced parameterization schemes, while able to reproduce the afternoon peak of maximum precipitation over most of the Amazon in contrast to the CMIP models, its spatial distribution is rather homogeneous and misses the nocturnal precipitation over the central and northeast Amazon.

The E-CON ensembles show evidence of OCS that are absent in the P-CON ensemble. These OCS are shown to be closely associated with the better representation of Amazon precipitation, as they explain the frequency of high intense rain rates and the heterogeneity of the precipitation diurnal cycle in observations. The similarity between E-CON and observations improves in both the distribution of precipitation intensity and diurnal cycle when only considering precipitation from OCS. However, the OCS simulated by the E-CON ensemble are still less frequent, smaller and more intense than observed.

The simulated and observed OCS cluster into nocturnal and diurnal systems. The environment of the nocturnal versus diurnal systems differs systematically. Nocturnal clusters are associated with stronger easterlies in the lower troposphere, peaking at about 850 hPa and forming part of the Amazonian low-level jet (Anselmo et al., 2020). In addition, an elevated cooler atmosphere propagates with the OCS during the early morning. Not surprisingly, the diurnal OCS show a stronger signature at the surface than the nocturnal OCS. The E-CON simulations suggest that cold pools contribute to the propagation of OCS in the northern Amazon and those that are very intense (D3-OCS). A composite analysis over diurnal clusters shows a strong temperature perturbation at the surface that propagates during the early afternoon. Given that the simulations produced about 20% less of diurnal OCS than observations, such systems may be sensitive to the representation of surface processes in ways that the E-CON simulations insufficiently capture. Likewise, the overestimation of nocturnal OCS relative to the diurnal OCS might be related to an inadequate representation of stratiform features by E-CON.

Our simulations show a clear improvement in many aspects of precipitation over the Amazon river basin when the precipitating systems are simulated explicitly. By simulating the geometry and transient dynamics of precipitating convection systems, a better representation of OCS emerges, and these prove essential for capturing many features of the observed precipitation over the Amazon. Nonetheless, our simulations also show room for improvement. For instance, in representing the relative prominence of organized systems during the day, which may be sensitive to land-surface processes, and in the timing of the nocturnal peak of precipitation, which has previously been shown to be sensitive to cloud microphysical processes (e.g., Feng et al., 2018). Simulations with a twofold finer grid do not lead to dramatic improvements, indicating that to the extent deficiencies are related to a poor representation of small-scale processes, capturing these effects explicitly would require much (hecto to deca meter) finer resolution.

Data Availability Statement

HadISST data (Rayner et al., 2003) is available at https://www.metoffice.gov.uk/hadobs/hadisst/data/download.html. CMORPH precipitation dataset were obtained from https://www.ncei.noaa.gov/data/cmorph-high-resolution-global-precipitation-estimates/access/30min/8km. Boundaries of the Amazon are available at Lehner et al. (2006) and were obtained from https://www.hydrosheds.org/products/hydrobasins. CMIP output of this study were replicated and made available for this study by the German Climate Computing Centre (Deutschen Klimarechenzentrum, DKRZ) at https://esgf-data.dkrz.de/projects/cmip6-dkrz/. Primary data and scripts used in the analysis that may be useful in reproducing the author's work are archived by the Max Planck Institute for Meteorology and can be obtained via the institutional repository https://pure.mpg.de.

Acknowledgments
This study was supported by the Max Planck Society for the Advancement of Science and the European Horizon 2020 project CONSTRAIN (project 493B). The authors thank Jaemyeong Seo for providing scripts for the cold pool detection and Cathy Hohenegger for her useful and constructive comments on the paper. The authors also thank the three anonymous reviewers for their valuable feedback. Open Access funding enabled and organized by Projekt DEAL.

References

Anselmo, E. M., Machado, L. A., Schumacher, C., & Kiladis, G. N. (2021). Amazonian mesoscale convective systems: Life cycle and propagation characteristics. *International Journal of Climatology*, *41*(7), 3968–3981. https://doi.org/10.1002/joc.7053

Anselmo, E. M., Schumacher, C., & Machado, L. A. (2020). The Amazonian low-level jet and its connection to convective cloud propagation and evolution. *Monthly Weather Review*, *148*(10), 4083–4099. https://doi.org/10.1175/mwr-d-19-0414.1

Arnold, N. P., Putman, W. M., & Freitas, S. R. (2020). Impact of resolution and parameterized convection on the diurnal cycle of precipitation in a global nonhydrostatic model. *Journal of the Meteorological Society of Japan. Series. II*, *98*(6), 1279–1304. https://doi.org/10.2151/jmsj.2020-066

Asensio, H., Messmer, M., Lüthi, D., & Osterried, K. (2020). External parameters for numerical weather prediction and climate application extpar v5_0 [Software]. User and Implementation Guide. Retrieved from: https://www.cosmo-model.org/content/support/software/ethz/EXTPAR_user_and_implementation_manual_202003.pdf

Bechtold, P. (2017). Atmospheric moist convection. *Meteorological Training Course Lecture Series*, 1–78. Retrieved from https://www.ecmwf.int/node/16953

Bechtold, P., Köhler, M., Jung, T., Doblas-Reyes, F., Leutbecher, M., Rodwell, M. J., et al. (2008). Advances in simulating atmospheric variability with the ECMWF model: From synoptic to decadal time-scales. *Quarterly Journal of the Royal Meteorological Society: A Journal of the Atmospheric Sciences, Applied Meteorology and Physical Oceanography*, *134*(634), 1337–1351. https://doi.org/10.1002/qj.289

Becker, T., Bechtold, P., & Sandu, I. (2021). Characteristics of convective precipitation over tropical Africa in storm-resolving global simulations. *Quarterly Journal of the Royal Meteorological Society*, *147*(741), 4388–4407. https://doi.org/10.1002/qj.4185

Betts, A. K., & Jakob, C. (2002). Study of diurnal cycle of convective precipitation over Amazonia using a single column model. *Journal of Geophysical Research*, *107*(D23), ACL25–ACL25-13. https://doi.org/10.1029/2002jd002264

Birch, C. E., Roberts, M. J., Garcia-Carreras, L., Ackerley, D., Reeder, M. J., Lock, A. P., & Schiemann, R. (2015). Sea-breeze dynamics and convection initiation: The influence of convective parameterization in weather and climate model biases. *Journal of Climate*, *28*(20), 8093–8108. https://doi.org/10.1175/jcli-d-14-00850.1

Burleyson, C. D., Feng, Z., Hagos, S. M., Fast, J., Machado, L. A., & Martin, S. T. (2016). Spatial variability of the background diurnal cycle of deep convection around the GoAmazon2014/5 field campaign sites. *Journal of Applied Meteorology and Climatology*, *55*(7), 1579–1598. https://doi.org/10.1175/jamc-d-15-0229.1

Chavez, S. P., & Takahashi, K. (2017). Orographic rainfall hot spots in the Andes-Amazon transition according to the TRMM precipitation radar and in situ data. *Journal of Geophysical Research: Atmospheres*, *122*(11), 5870–5882. https://doi.org/10.1002/2016jd026282

Crook, J., Klein, C., Folwell, S., Taylor, C. M., Parker, D. J., Stratton, R., & Stein, T. (2019). Assessment of the representation of West African storm lifecycles in convection-permitting simulations. *Earth and Space Science*, *6*(5), 818–835. https://doi.org/10.1029/2018ea000491

Doms, G., Förstner, J., Heise, E., Herzog, H., Mironov, D., Raschendorfer, M., et al. (2011). A description of the nonhydrostatic regional cosmo model. Part II: Physical parameterization. *Cosmo*, *154*. http://www.cosmo-model.org

Eyring, V., Bony, S., Meehl, G. A., Senior, C. A., Stevens, B., Stouffer, R. J., & Taylor, K. E. (2016). Overview of the coupled model Intercomparison project phase 6 (CMIP6) experimental design and organization. *Geoscientific Model Development*, *9*(5), 1937–1958. https://doi.org/10.5194/gmd-9-1937-2016

Feng, Z., Leung, L. R., Houze, R. A., Jr., Hagos, S., Hardin, J., Yang, Q., et al. (2018). Structure and evolution of mesoscale convective systems: Sensitivity to cloud microphysics in convection-permitting simulations over the United States. *Journal of Advances in Modeling Earth Systems*, *10*(7), 1470–1494. https://doi.org/10.1029/2018ms001305

Feng, Z., Leung, L. R., Liu, N., Wang, J., Houze, R. A., Jr., Li, J., et al. (2021). A global high-resolution mesoscale convective system database using satellite-derived cloud tops, surface precipitation, and tracking. *Journal of Geophysical Research: Atmospheres*, *126*(8), e2020JD034202. https://doi.org/10.1029/2020jd034202

Fiedler, S., Crueger, T., D'Agostino, R., Peters, K., Becker, T., Leutwyler, D., et al. (2020). Simulated tropical precipitation assessed across three major phases of the Coupled Model Intercomparison Project (CMIP). *Monthly Weather Review*, *148*(9), 3653–3680. https://doi.org/10.1175/mwr-d-19-0404.1

Fitzjarrald, D. R., Sakai, R. K., Moraes, O. L., De Oliveira, R. C., Acevedo, O. C., Czikowsky, M. J., & Beldini, T. (2008). Spatial and temporal rainfall variability near the Amazon-tapajós confluence. *Journal of Geophysical Research*, *113*(G1). https://doi.org/10.1029/2007jg000596

Gao, X., Xu, Y., Zhao, Z., Pal, J., & Giorgi, F. (2006). On the role of resolution and topography in the simulation of East Asia precipitation. *Theoretical and Applied Climatology*, *86*(1), 173–185. https://doi.org/10.1007/s00704-005-0214-4

Garreaud, R., & Wallace, J. M. (1997). The diurnal march of convective cloudiness over the Americas. *Monthly Weather Review*, *125*(12), 3157–3171. https://doi.org/10.1175/1520-0493(1997)125<3157:tdmocc>2.0.co;2

Garstang, M., Massie, H. L., Jr., Halverson, J., Greco, S., & Scala, J. (1994). Amazon coastal squall lines. Part I: Structure and kinematics. *Monthly Weather Review*, *122*(4), 608–622. https://doi.org/10.1175/1520-0493(1994)122<0608:acslpi>2.0.co;2

Greco, S., Swap, R., Garstang, M., Ulanski, S., Shipham, M., Harriss, R., et al. (1990). Rainfall and surface kinematic conditions over central Amazonia during ABLE 2B. *Journal of Geophysical Research*, *95*(D10), 17001–17014. https://doi.org/10.1029/jd095id10p17001

Heise, E., Ritter, B., Schrodin, R., & Wetterdienst, D. (2006). Operational implementation of the multilayer soil model. *Citeseer*.

Herbert, R., Stier, P., & Dagan, G. (2021). Isolating large-scale smoke impacts on cloud and precipitation processes over the amazon with convection permitting resolution. *Journal of Geophysical Research: Atmospheres*, *126*(13). https://doi.org/10.1029/2021jd034615

Hirt, M., Craig, G. C., Schäfer, S. A., Savre, J., & Heinze, R. (2020). Cold-pool-driven convective initiation: Using causal graph analysis to determine what convection-permitting models are missing. *Quarterly Journal of the Royal Meteorological Society*, *146*(730), 2205–2227. https://doi.org/10.1002/qj.3788

Holloway, C., Woolnough, S., & Lister, G. (2012). Precipitation distributions for explicit versus parametrized convection in a large-domain high-resolution tropical case study. *Quarterly Journal of the Royal Meteorological Society*, *138*(668), 1692–1708. https://doi.org/10.1002/qj.1903

Houze, R. A., Jr. (2004). Mesoscale convective systems. *Reviews of Geophysics*, *42*(4). https://doi.org/10.1029/2004rg000150

Houze, R. A., Jr., Rasmussen, K. L., Zuluaga, M. D., & Brodzik, S. R. (2015). The variable nature of convection in the tropics and subtropics: A legacy of 16 years of the tropical rainfall measuring mission satellite. *Reviews of Geophysics*, *53*(3), 994–1021. https://doi.org/10.1002/2015rg000488

Inoue, T., Rajendran, K., Satoh, M., & Miura, H. (2021). On the semidiurnal variation in surface rainfall rate over the tropics in a global cloud-resolving model simulation and satellite observations. *Journal of the Meteorological Society of Japan. Series II*, *99*(5), 1371–1388. https://doi.org/10.2151/jmsj.2021-066

Janowiak, J. E., Kousky, V. E., & Joyce, R. J. (2005). Diurnal cycle of precipitation determined from the CMORPH high spatial and temporal resolution global precipitation analyses. *Journal of Geophysical Research*, *110*(D23), D23105. https://doi.org/10.1029/2005jd006156

Judt, F., & Rios-Berrios, R. (2021). Resolved convection improves the representation of equatorial waves and tropical rainfall variability in a global nonhydrostatic model. *Geophysical Research Letters*, *48*(14). https://doi.org/10.1029/2021gl093265

Junquas, C., Takahashi, K., Condom, T., Espinoza, J.-C., Chávez, S., Sicart, J.-E., & Lebel, T. (2018). Understanding the influence of orography on the precipitation diurnal cycle and the associated atmospheric processes in the central andes. *Climate Dynamics*, *50*(11), 3995–4017. https://doi.org/10.1007/s00382-017-3858-8

Lehner, B., Verdin, K., & Jarvis, A. (2006). Hydrological data and maps based on Shuttle elevation derivatives at multiple scales (HydroSHEDS)-technical documentation Dataset. *World Wildlife Fund US*.

Love, B. S., Matthews, A. J., & Lister, G. M. (2011). The diurnal cycle of precipitation over the maritime continent in a high-resolution atmospheric model. *Quarterly Journal of the Royal Meteorological Society*, *137*(657), 934–947. https://doi.org/10.1002/qj.809

Mapes, B., & Neale, R. (2011). Parameterizing convective organization to escape the entrainment dilemma. *Journal of Advances in Modeling Earth Systems*, *3*(2). https://doi.org/10.1029/2011ms000042

Marengo, J. A. (2006). On the hydrological cycle of the amazon basin: A historical review and current state-of-the-art. *Revista brasileira de meteorologia*, *21*(3), 1–19.

Mlawer, E. J., Taubman, S. J., Brown, P. D., Iacono, M. J., & Clough, S. A. (1997). Radiative transfer for inhomogeneous atmospheres: Rrtm, a validated correlated-k model for the longwave. *Journal of Geophysical Research*, *102*(D14), 16663–16682. https://doi.org/10.1029/97jd00237

Paccini, L., Hohenegger, C., & Stevens, B. (2021). Explicit versus parameterized convection in response to the Atlantic meridional mode. *Journal of Climate*, *34*(9), 3343–3354. https://doi.org/10.1175/jcli-d-20-0224.1

Pereira Filho, A. J., Carbone, R. E., Tuttle, J. D., & Karam, H. A. (2015). Convective rainfall in Amazonia and adjacent tropics. *Atmospheric and Climate Sciences*, *5*(02), 137–161. https://doi.org/10.4236/acs.2015.52011

Phillips, O. L., Lewis, S. L., Baker, T. R., Chao, K.-J., & Higuchi, N. (2008). The changing amazon forest. *Philosophical Transactions of the Royal Society B: Biological Sciences*, *363*(1498), 1819–1827. https://doi.org/10.1098/rstb.2007.0033

Prein, A. F., Langhans, W., Fosser, G., Ferrone, A., Ban, N., Goergen, K., et al. (2015). A review on regional convection-permitting climate modeling: Demonstrations, prospects, and challenges. *Reviews of Geophysics*, *53*(2), 323–361. https://doi.org/10.1002/2014rg000475

Prill, F. (2020). DWD ICON tools documentation (Tech. Rep.). Software. *Deutscher Wetterdienst (DWD)*.

Raschendorfer, M. (2001). The new turbulence parameterization of LM. COSMO News Letter No. 1. *Consortium for Small-Scale Modelling*, 89–97. Retrieved from http://www.cosmo-model.org

Rayner, N., Parker, D. E., Horton, E., Folland, C. K., Alexander, L. V., Rowell, D., & Kaplan, A. (2003). Global analyses of sea surface temperature, sea ice, and night marine air temperature since the late nineteenth century [Dataset]. Journal of Geophysical Research, *108*(D14).4407. https://doi.org/10.1029/2002jd002670

Rehbein, A., Ambrizzi, T., & Mechoso, C. R. (2018). Mesoscale convective systems over the Amazon basin. Part I: Climatological aspects. *International Journal of Climatology*, *38*(1), 215–229. https://doi.org/10.1002/joc.5171

Richter, I., & Xie, S.-P. (2008). On the origin of equatorial Atlantic biases in coupled general circulation models. *Climate Dynamics*, *31*(5), 587–598. https://doi.org/10.1007/s00382-008-0364-z

Rickenbach, T. M. (2004). Nocturnal cloud systems and the diurnal variation of clouds and rainfall in southwestern Amazonia. *Monthly Weather Review*, *132*(5), 1201–1219. https://doi.org/10.1175/1520-0493(2004)132<1201:ncsatd>2.0.co;2

Rousseeuw, P. J. (1987). Silhouettes: A graphical aid to the interpretation and validation of cluster analysis. *Journal of Computational and Applied Mathematics*, *20*, 53–65. https://doi.org/10.1016/0377-0427(87)90125-7

Santos, M. J., Medvigy, D., Silva Dias, M. A., Freitas, E. D., & Kim, H. (2019). Seasonal flooding causes intensification of the river breeze in the central amazon. *Journal of Geophysical Research: Atmospheres*, *124*(10), 5178–5197. https://doi.org/10.1029/2018jd029439

Sato, T., Miura, H., Satoh, M., Takayabu, Y. N., & Wang, Y. (2009). Diurnal cycle of precipitation in the tropics simulated in a global cloud-resolving model. *Journal of Climate*, *22*(18), 4809–4826. https://doi.org/10.1175/2009jcli2890.1

Satoh, M., Stevens, B., Judt, F., Khairoutdinov, M., Lin, S.-J., Putman, W. M., & Düben, P. (2019). Global cloud-resolving models. *Current Climate Change Reports*, *5*(3), 172–184. https://doi.org/10.1007/s40641-019-00131-0

Slingo, J., Bates, P., Bauer, P., Belcher, S., Palmer, T., Stephens, G., et al. (2022). Ambitious partnership needed for reliable climate prediction. *Nature Climate Change*, *12*(6), 499–503. https://doi.org/10.1038/s41558-022-01384-8

Stephens, G. L., L'Ecuyer, T., Forbes, R., Gettelmen, A., Golaz, J.-C., Bodas-Salcedo, A., et al. (2010). Dreary state of precipitation in global models. *Journal of Geophysical Research*, *115*(D24). https://doi.org/10.1029/2010jd014532

Stevens, B., Acquistapace, C., Hansen, A., Heinze, R., Klinger, C., Klocke, D., et al. (2020). The added value of large-eddy and storm-resolving models for simulating clouds and precipitation. *Journal of the Meteorological Society of Japan. Series II*, *98*(2), 395–435. https://doi.org/10.2151/jmsj.2020-021

Tai, S.-L., Feng, Z., Ma, P.-L., Schumacher, C., & Fast, J. D. (2021). Representations of precipitation diurnal cycle in the amazon as simulated by observationally constrained cloud-system resolving and global climate models. *Journal of Advances in Modeling Earth Systems*, *13*(11), e2021MS002586. https://doi.org/10.1029/2021ms002586

Tanaka, L. d. S., Satyamurty, P., & Machado, L. A. T. (2014). Diurnal variation of precipitation in central Amazon Basin. *International Journal of Climatology*, *34*(13), 3574–3584. https://doi.org/10.1002/joc.3929

Tang, S., Gleckler, P., Xie, S., Lee, J., Ahn, M.-S., Covey, C., & Zhang, C. (2021). Evaluating the diurnal and semidiurnal cycle of precipitation in CMIP6 models using satellite-and ground-based observations. *Journal of Climate*, *34*(8), 3189–3210.

Vergara-Temprado, J., Ban, N., Panosetti, D., Schlemmer, L., & Schär, C. (2020). Climate models permit convection at much coarser resolutions than previously considered. *Journal of Climate*, *33*(5), 1915–1933. https://doi.org/10.1175/jcli-d-19-0286.1

Web Services of Deutscher Wetterdienst. (2021). Retrieved from https://webservice.dwd.de/cgi-bin/spp1167/webservice.cgi. Accessed 20210607.

Wu, M., Lee, J.-E., Wang, D., & Salameh, M. (2021). Suppressed daytime convection over the Amazon river. *Journal of Geophysical Research: Atmospheres*, *126*(13), e2020JD033627. https://doi.org/10.1029/2020jd033627

Xie, P., Joyce, R., Wu, S., Yoo, S.-H., Yarosh, Y., Sun, F., & Lin, R. (2017). Reprocessed, bias-corrected CMORPH global high-resolution precipitation estimates from 1998 [Dataset]. Journal of Hydrometeorology, *18*(6), 1617–1641. https://doi.org/10.1175/jhm-d-16-0168.1

Yang, S., Kuo, K.-S., & Smith, E. A. (2008). Persistent nature of secondary diurnal modes of precipitation over oceanic and continental regimes. *Journal of Climate*, *21*(16), 4115–4131. https://doi.org/10.1175/2008jcli2140.1

Yashiro, H., Kajikawa, Y., Miyamoto, Y., Yamaura, T., Yoshida, R., & Tomita, H. (2016). Resolution dependence of the diurnal cycle of precipitation simulated by a global cloud-system resolving model. *Sola*, *12*(0), 272–276. https://doi.org/10.2151/sola.2016-053

Yin, L., Fu, R., Shevliakova, E., & Dickinson, R. E. (2013). How well can CMIP5 simulate precipitation and its controlling processes over tropical south America? *Climate Dynamics*, *41*(11–12), 3127–3143. https://doi.org/10.1007/s00382-012-1582-y

Zängl, G., Reinert, D., Rípodas, P., & Baldauf, M. (2015). The ICON (ICOsahedral Non-hydrostatic) modelling framework of DWD and MPI-M: Description of the non-hydrostatic dynamical core. *Quarterly Journal of the Royal Meteorological Society*, *141*(687), 563–579. https://doi.org/10.1002/qj.2378